Analysis of the Final States $\pi^0\eta$ and $\eta\eta$ in $\overline{p}p$ - Annihilation in Flight

Bachelorarbeit

im
Studiengang
„Bachelor of Science“
im Fach Physik

an der Fakultät für Physik und Astronomie
der Ruhr-Universität Bochum

von
Haroutioun Ohannessian

aus
Yerevan

Bochum 2011

Contents

1 Introduction

From the start of History people have been asking a question, that has till today motivated many people to keep on searching and pushing our knoweldge a step closer to finding an answer. “What is our world made of?”. One of the pioneeres who set a stepping-stone for modern discoveries was Mendeleev. He wrote a simple table called “The Periodic Table” which included chemical elements that our world was made of. The Mendeleev’s table had only one problem it wasn’t complete and simple enough to represent the “ultimate” solution. We now know that these elements are built up of more fundemental particles called electrons, protons and neutrons. The protons and neutrons which together are labeled as nucleons, are “glued” together with a strong nuclear force to form the nuclei. These are subsequently bound by electrons through the electromagnetic force to form the atom(different numbers of electrons and nucleons form different atoms). Then it was observed that through the conversion of neutrons into protons by *weak interactions* a ray is produced which we now know as the β-ray(the process is called β-decay).

With time scientists discovered that neutrons and protons are not the only existing particles, but rather a portion of a group of particles called the *baryons*. The name baryon means“heavy” in the greek language. It was given that name, because at the time of their discovery most other particles were lighter than the baryons. Another group of particles which has been discovered are the *mesons*(which we will look at in more detail in the section 1.2). These two groups the baryons and mesons undergo strong interactions, so they together are known as the *hadrons*.

To understand hadrons and their interactions, scientists need to perform experiments. One of these experiments is known as the $\overline{P}$ANDA [1] experiment, which will give us a better understanding of hadrons and their interactions via Antiproton-proton annihilation processes.

1.1 Quantum Chromodynamics

Despite the amazing progress made in the last decades in the field of particle physics, we still have a vague understanding in some fields of the strong interactions(non perturbative quantum chromodynamics is still not fully understood). The theory that describes it in the standard model is called *quantum chromodynamics*, or QCD. All elementary particles are either *bosons* or *fermions*. The interactions are mediated through bosons and are called *gauge bosons*; which are *photons*(force carriers of the electromagnetic field), W

[1] anti*P*roton *An*nihilation at *Da*rmstadt

and Z bosons(force carriers of the weak interactions) and *gluons*(force carriers of the strong interactions).

Since this thesis includes strong interactions it is important to know that gluons are massless spin-1 bosons that have zero electric charge. Due to the fact that they couple to to colour charges the gluons are self interacting particles. A free particle then would be colourless, which actually means that the total colour of the combined quarks adds up to “white”. This explains why we haven’t found a quark as a free particle and is known as the confinment thoery. So if we had to summerize this idea the easiest way to put it in words would be that “quarks interact strongly by exchanging colours”.

1.2 Mesons

Conventional mesons are particles composed of one quark and one anti-quark. These two quarks are bound together through strong interaction. All mesons are unstable and depending on the interaction of the decay have a lifetime between 10^{-8} to 10^{-24} seconds. Since the final states in this thesis are composed of mesons it is important to take a bit of time to understand what kind of decays they can undergo.

Mesons can decay into lighter hadrons, leptons or photons. The decay we will see here is the most basic one, where a neutral meson decays into two photons.

You might ask yourself how are mesons produced? Well there are natural existing mesons like when a very high energy interaction takes place between two particles (example: cosmic ray interactions). Artificially produced mesons also exist in high-energy particle accelerators that collide two particles(In our case we have a proton anti-proton annihilation). The mesons produced that are relevent in this thesis are stated in table 1.1.

Meson type	Symbol	J^p	I	Mass [Mev/c^2]	Mean Lifetime [s]	Decay mode
pseudoscalar meson	$\pi^{\pm}$	0^-	1	139,6	$2,6 \cdot 10^{-8}$	$\mu^{\pm}\ \nu_\mu \approx 100\%$
pseudoscalar meson	π^0	0^-	1	135,0	$8,4 \cdot 10^{-16}$	$2\gamma \approx 99\%$
pseudoscalar meson	η	0^-	0	547,3	$5,5 \cdot 10^{-19}$	$2\gamma \approx 39\%$ $3\pi^0 \approx 32,51\%$
pseudoscalar meson	η'	0^-	0	957,8	$3,3 \cdot 10^{-21}$	$\pi^0\pi^0\eta \approx 65\%$ $\pi^0\gamma \approx 30\%$
vector meson	ω	1^-	0	781,9	$2,6 \cdot 10^{-23}$	$3\pi^0 \approx 89\%$

Table 1.1: Some mesons and their properties

Let’s now take a look at the mesons that are important to us:

π^0-**Meson** was one of the first hadrons discovered(after the proton and neutron). The discovery of the pion was not unexpected, since Yukawa had predicted their existance and their approximate masses. The pions are the lightest known mesons and their quark composition is as follows:

$$\left|\pi^0\right\rangle = \frac{\left|u\overline{u}\right\rangle - \left|d\overline{d}\right\rangle}{\sqrt{2}} \left|\pi^+\right\rangle = \left|u\overline{d}\right\rangle \left|\pi^-\right\rangle = \left|d\overline{u}\right\rangle$$

η-**Meson** are made of a mixture of up, down and strange quarks and their antiquarks. The η meson was discovered in pion-nucleon collisions at the Bevatron in 1961. It's composition is as follows:

$$\left|\eta\right\rangle = \frac{\left|u\overline{u}\right\rangle + \left|d\overline{d}\right\rangle - \left|2s\overline{s}\right\rangle}{\sqrt{6}}$$

Both the π^0 and the η particles are also their own antiparticles.

Next to the conventional mesons there are also exotic mesons, which consist of an additional $q\overline{q}$-pairs or gluonic degrees of freedom. The additional degrees of freedom carried by gluons allow these hybrids and glueballs to have J^PC exotic quantum numbers. Glueballs consists solely of gluon particles. Such a state is possible because gluons carry color charge and experience the strong interaction. Glueballs are extremely difficult to identify in particle accelerators, because they mix with ordinary meson states. One major physics program of the future $\overline{P}$ANDA experiment will be the search of various exotic states and the search for gluonic excitations.

1.3 $\overline{P}$ANDA-Experiment

The study of hadronic resonances, hadron spectroscopy and weak- strong interactions are some of the fields of research elaborated with $\overline{P}$ANDA. This experiment will take place at the Facility for Antiproton and Ion Research(FAIR) Figure 1.1, currently under construction in Darmstadt, Germany. The goal is to perform the experiment at a very high precision level (never done before). This aspiring goal might be reached through a Fixed-Target-Experiment, where the detector has a very high energy and spatial resolution, with almost complete 4π angle coverage. Antiproton-proton-annihilations will take place inside the detector, which gives a very favourable enviroment to study different hadron states with several quantum numbers. The antiproton beam needed for such experiments has to be of high quality [2] and it will have to provide a luminosity of $2\cdot10^{32}/\text{cm}^2\text{s}$. The beam will be produced in the FAIR accelerator complex and stored in a High Energy Storage Ring(HESR)which passes through the detector with a momentum of 1,5 GeV/c to 15 GeV/c. To have a good momentum resolution the detector is split into two spectrometer parts Fig. 1.2. One being the *target spectrometer*, equipped with a superconducting solenoid magnet measuring at high angles. The other being the *forward spectrometer* a dipole magnet for small angle tracks. A silicon vertex detector surrounds the interaction point. In both spectrometer parts, tracking charged particle

[2] momentum-resolution:$\sigma/p \approx 2\cdot10^{-5}$ till 10^{-4}

identification done by the gas- and drift chamber, electromagnetic calorimetry(which allows us to detect photons)and muon identification through the muon detector are made possible.

1.4 Motivation

In this thesis data collected from the Crystal-Barrel experiment will be analyzed. The reason behind this experiment was to get new information about the light meson spectrum, which can be done through $p\overline{p}$-Annihilations. As mentioned before we will be looking at the two following final states:

$$p\overline{p} \rightarrow \pi^0\eta \rightarrow 4\gamma$$
$$p\overline{p} \rightarrow \eta\eta \rightarrow 4\gamma$$

The initial $\overline{p}$ momentumes that we will look at are 900 MeV/c and 1800 MeV/c. In this thesis the angular distributions of the scalar mesons in the CM (center of mass) system of the $p\overline{p}$ reaction of the two channels stated above are of great interest. Since these angular distributions obtain direct information about the contributing initial spin waves. These will provide a better understanding of the $p\overline{p}$ annihilation mechanisem. With a further partial wave analysis it is possible to determine the maximum momenta of the initial state and in addition to identify resonances in the $p\overline{p}$ formation. Also these states can help in the caliberation of the EMC of $\overline{P}$ANDA (electromagnetic calorimeter).

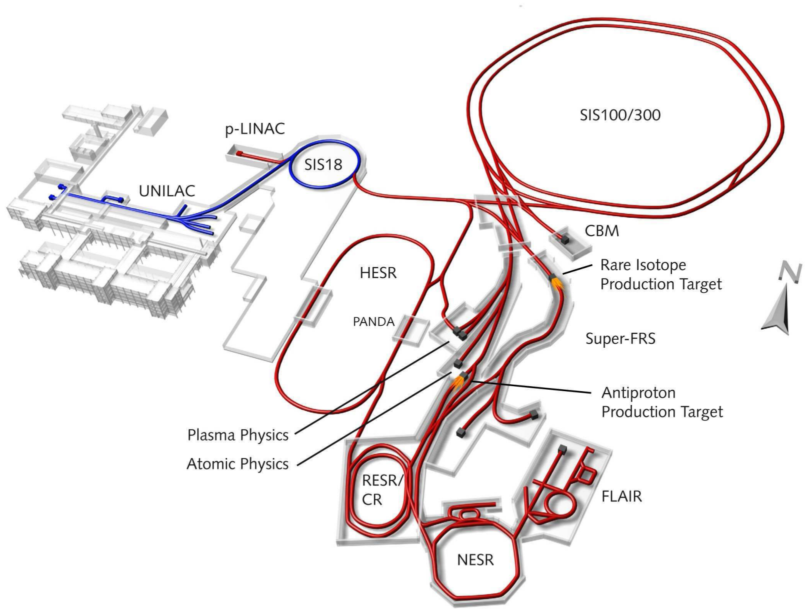

Figure 1.1: The accelerator complex of FAIR

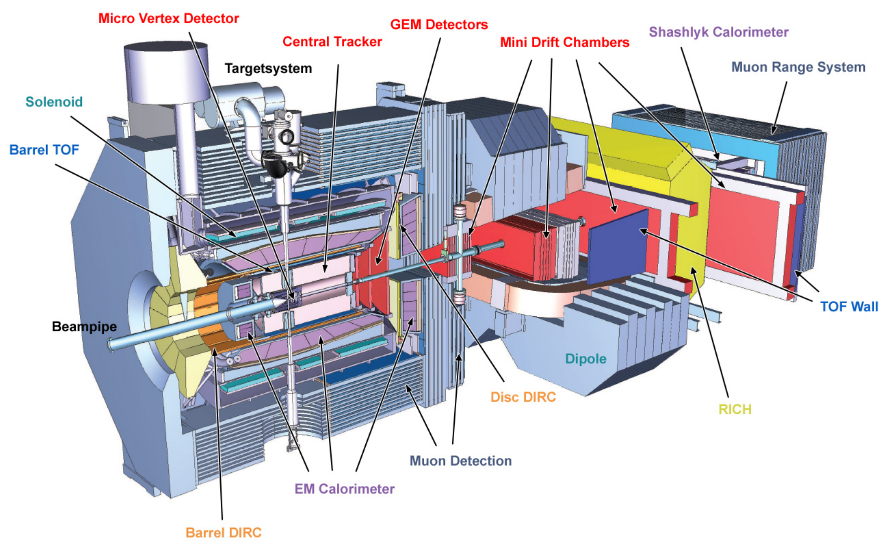

Figure 1.2: Target- and forward spectrometer of the PANDA detector

2 The Crystal Barrel Experiment

The Crystal Barrel experiment ran at the LEAR [1], from 1989 till 1996 and studied $\overline{p}p$ annihilations both at rest and in flight. The detector is a nearly 4π, high resolution system for both charged particles and photons. One of the main goals of the experiment was to search for gluonic exciations in the meson spectrum. This includes both glueballs, and hybrid mesons.

2.1 Antiproton Production

The low energy antiproton ring is situated in CERN, in the southern part of the PS[2](Fig. 2.1). This facility enables the production of intense beams of antiproton. The antiprotons are extracted from the antiproton accumulator at a momentum of 3,5 GeV/c, which are then decelerated in the PS to 0,6 GeV/c and afterwards injected in the LEAR.

LEAR ejects $10^6 p/s$ with a slow period of $10^3 s$. The momentum of the antiproton beam is then adjusted between 0,1 and 2 GeV/c. For annihilations in flight the antiproton rate is increased to $3 \cdot 10^5 p/s$ (the equivalent annihilation at rest needs around $3000 p/s$).

2.2 Crystal Barrel Detector

The Crystal Barrel detector was the first low energy 4π detector that took high precision measurements of charged mesons and photons simultaneously. Antiprotons from LEAR enter the detector along the axis of a solenoidal magnetic field of 1,5 T (Fig. 2.2). Low momentum antiprotons (0,2 GeV/c) lose energy through ionization and stop in the middle of the 44mm long liquid hydrogen target.

At higher momentum only a small amount of the antiprotons annihilate. The rest pass through the target without interacting with it. For this reason a second counter is situated behind the target. So the signal of the front counter with a missing signal in the back counter means an annihilation took place (ex.: if 4 signals were registered at the front and 2 signals at the back that means 2 annihilations took place). There is also the additional reaction that can take place during the opening of the gate circuits, this is due to the high rate of the incoming antiprotons. This type of event is called *pile up*.

As seen in (Fig 2.2) the Crystal-Barrel detector is a multi-component detector system made of the following components:

[1]**L**ow **E**nergy **A**ntiproton **R**ing
[2]**P**roton **S**ynchrotron

- Target (liquid hydrogen, hydrogen gas, liquid deuterium)
- Silicon-Vertex Detector
- Jet-Drift Chamber
- Electromagnetic Calorimeter
- Trigger System

2.2.1 Silicon-Vertex Detector

The inner part of the detector surrounding the target was replaced by a silicon microstrip detector in 1994 (before that the proportional wire chamber was used). It was constructed to improve the momentum and vertex resolution of the tracks originating within the target. It consists of 15 overlapping modules of 128 microstrips each. They are positioned at a distance of 4 mm from the target.

2.2.2 Jet-Drift Chamber

The jet drift chamber surrounds the silicon vertex detector. It measures 40 cm long, and 40 cm in diameter. It is divided into 30 sectors, each of which contains 23 layers of sense wires. The basic way it functions is that the particles travel through the chamber which is filled with gas. The gas is then ionized by the passage of the particle. Ionization drifts and diffuses in an electric and magnetic field towards an electrode. The anode signal is then collected and amplified, and the charge induced on the cathode creates detectible signals. Finally the measurement of the trajectory determines the particle momentum.

2.2.3 Electromagnetic Calorimeter

The electromagnetic calorimeter is made of a barrel containing 1380 crystals. The crystals are grouped in 26 rings, where the large rings cover 6° in both azimuthal and polar angles. The six smallest rings close to the beam axis contain 30 crystals and cover an angle of 12°. This gives the calorimeter an angle coverage of 97,8% of the 4π (Figure 2.3). The crystals consist of CsI doped with thallium and have high resolution photon detection properties. They are 30cm long and have a cross section of 2x2 cm^2 which allow the detection of photons in the energy range of 20 - 2000 MeV(Figure 2.4). Every crystal is covered in a $10\mu m$ titanium and is suspended on the inner aluminum wall.

The dominant absorption process for a hitting photon is the *pair production*. Since the electrons and positrons interact with the crystals mainly by the *bremsstrahlung*, the initial photon will lead to a cascade of e^+/e^- pairs and other photons(particle shower). This process continues till the energies of the secondary particles produced fall below the critical energy. The resulting photons go through a photomultiplier and then are transfered to an electric signal. With high photon energies the shower can reach the neighbouring crystal. So to be able to identify the original energy and position of the particle, the "active" crystals are summed to a so called *cluster*. Then a search for an energy peak in these clusters is performed and through caliberation constants the deposited photon energy can be calculated. The direction of the momentum is then deduced through the position of the cluster.

One problem that is encountered is the background noise that comes due to the read-out electronics. To get rid of this a default minimum energy value is set for the crystals. If this value is not reached then the crystal will not be evaluated. Due to the electromagnetic showers being characterized as a statistical process there could be more than one local maxima. This fluctuation can become so great that it gives rise to more than one cluster to be affected. This is known as an electromagnetic *splitoff*. This causes wrong reconstruction of photons. Here the use of a default minimum energy as a lower limit is not possible, because some of the low energy photons will then be lost. Therfore to be able to sperate the splitoffs from the photons artificial neural networks are used. There is also a second type of splitoff know as the *hadron splitoff*. This is like the electromagnteic splitoff except that here the splitoff is caused by a charged paticle.

The standard minimum energy value is 1 MeV. The crystals below this energy value will be ignored. A standard minimum value for a cluster is 10 MeV. Also a crystal inside a cluster must have a minimum energy of 4 MeV, so that it can be used as a starting point for the reconstruction software. The central crystal of a local energy maximum should have a value above 10 MeV so that it can be considered as an energy deposit for an independent particle. Such an energy maximum is called a PED [3].

2.2.4 Trigger System

There are three different level triggers that are used to minimize the dead time during data acquisition.

- **Level 0** trigger to check that the detector parts are all operational, this is done when no antiproton beam is present. The source of this trigger can be replaced by using additional light pulsers.
- **Level 1** trigger combines the information of the level 0 trigger with the charge multiplicity that comes from the JDC [4].
- **Level 2** trigger is a software trigger that uses the information of the CsI crystals to enhance final states mainly containing π^0 and η. That's why a search for a local maxima in the energy deposition of all the crystals, and a calculation of the photon energies and of the invariant masses of $\pi^0 \to \gamma\gamma$, $\eta \to \gamma\gamma$ is performed.

When the required trigger conditions are satisfied, the data bank will be filled with the remaining information of the event.For more information about the trigger system refer to [2].

[3] **P**article **E**nergy **D**eposit
[4] **J**et **D**rift **C**hamber

2.3 Offline Software

During the planning phase Monte-Carlo based simulations are used to address (look at) complex problems. For example the development and optimization of the individual detectors and hardware components. These simulations provide the experimenter information about the results that his experiment will give in advance. For the LEAR experiment this means that a desired decay can be simulated and evaluated, so that it might be put to use when the real experiments take place. This subjects the detectors to a constant improvment.

How useful such simulations are, depends on how close the simulation can get to the real experiment. For the LEAR experiment there are a collection of tools that are made available for use. To be able to simulate and evaluate data software packages are needed. Some of these softwares are important for this thesis and so it is important to have an understanding of how things work.

Event Generation takes place with the help of EvtGen[1]. It basically generates four-vectors of the particles in the final states, according to a given decay channel. For our study the following reactions are generated $p\overline{p} \rightarrow \pi^0\eta \rightarrow 4\gamma$, $p\overline{p} \rightarrow \eta\eta \rightarrow 4\gamma$.

Particle Propagation through the detector is simulated using the LOCATOR[3], BCTRACK[4] and GTRACK[5]. The LOCATOR is a chamber reconstruction software, the BCTRACK is the Crystal data reconstruction software and the GTRACK is the global tracking reconstruction software. The Monte Carlo events and its interaction with the Material is simulated by using GEANT3[6]. It simulates the passage of a particle through matter. This involves considering possible interactions and decay processes, and it also simulates the detector response by recording when a particle passes through the volume of a detector, and approximating how a real detector would respond.

Data Analysis is done by the help of CbOFF++ [7](Offline reconstruction software), CBKFIT [8](Calculation of kinematic fits) and ROOT [9](Powerful analysis software).

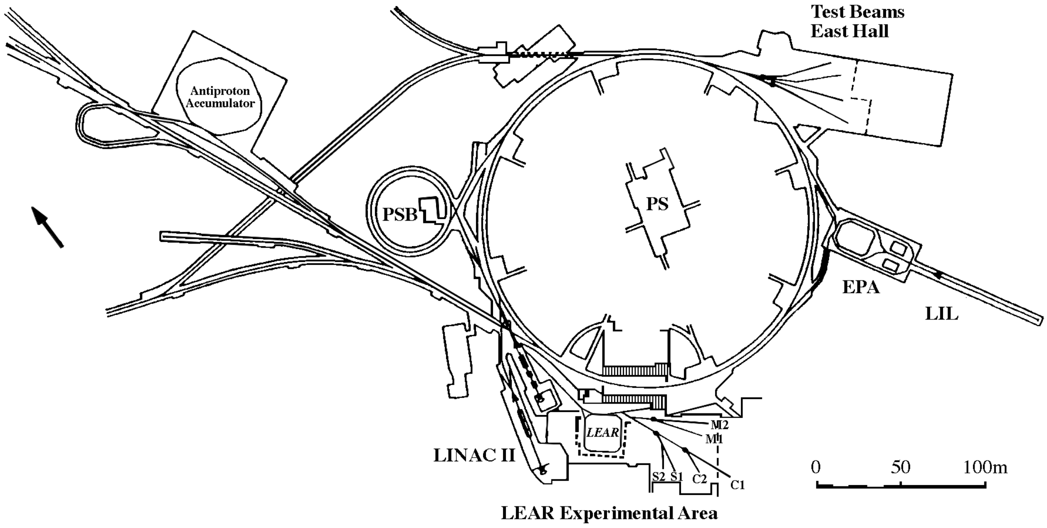

Figure 2.1: CERN Proton Synchrotron. Crystal Barrel Experiment is located at (C2)

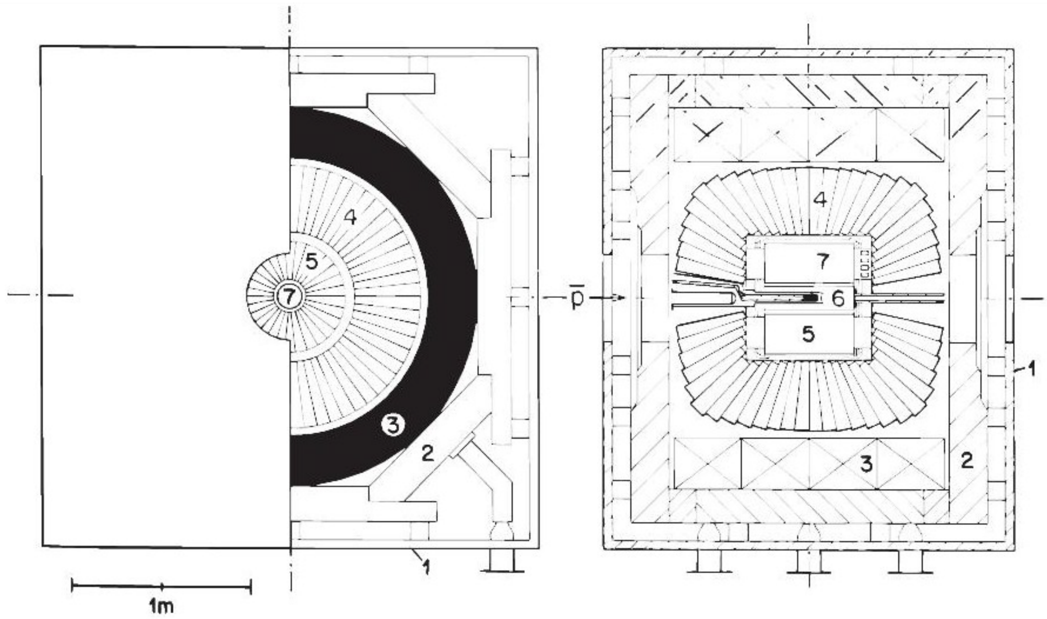

Figure 2.2: Side and front view of the Crystal Barrel detector. (1)Shielding (2)Magnet Yoke (3)Magnet Coils (4)Calorimeter (5)Jet-Drift Chamber (6)Silicon Vertex Detector (7)Target

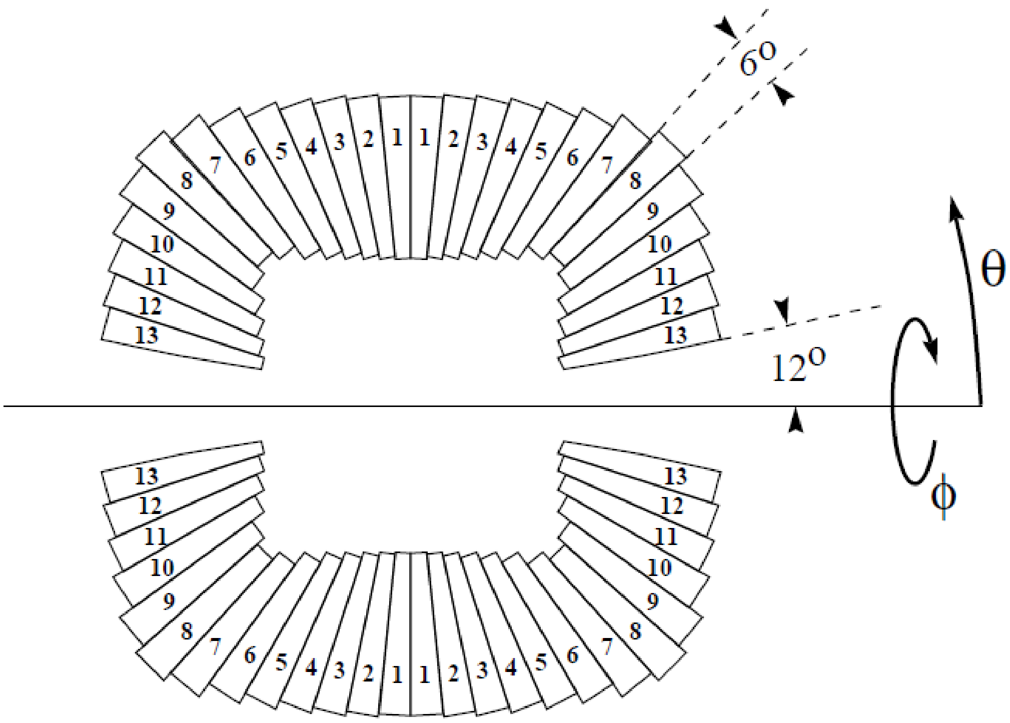

Figure 2.3: Cross section view of the electromagnetic calorimeter. Covered range is $12^o \leq \theta \leq 168^o$.

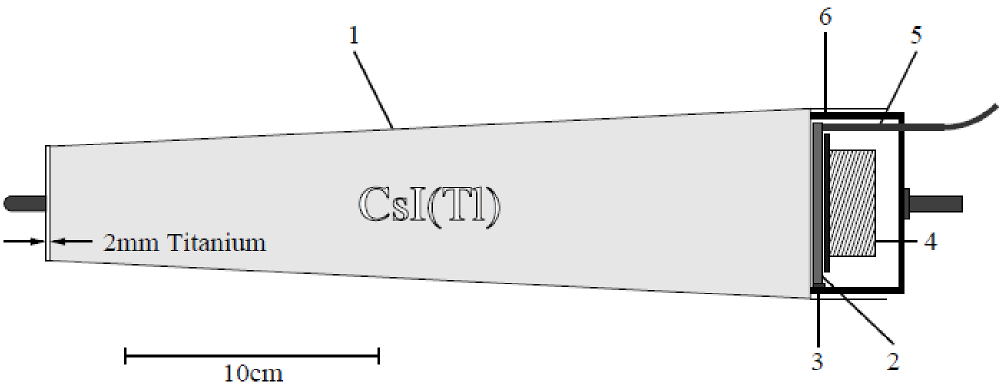

Figure 2.4: Cross section view of a CsI crystal. (1)Titanium (2)Wavelenght Shifter (3)Photodiode (4)preamplifier (5)Light Fiber (6)Brass Cover

3 Data Selection and Kinematic Fit

The data selection is made of stages that build on top of each other. There is the preselection(section 3.1), which narrows down the number of events that come through by applying rough cuts. Then comes the specific channel selection, which in our case is the $\pi^0\eta$ and $\eta\eta$ channels.

In particle physics it is often the case that when researching a certain channel or final state there are going to be other unwanted background events that are going to be produced. These by-products are decays that take place at a time where they are unwanted. So for example when looking at the $\pi^0\eta$ channel one can observe that there are certain events coming through which do not belong to the Final state $\pi^0\eta$ like for example $\pi^0\pi^0$ events. Our goal is then to perform a "cut" that will allow us to minimize these background channels without loosing valuable information. This is mainly accomplished through cuts on the CL[1].

So to be able to perform such cuts. Monte-Carlo events need to be generated, which can be done using GEANT3 simulation program. The program takes into consideration all the secondary processes of both active and passive parts of the detector. For photons this means pair production, compton scattering and photo-electric effect.

On top of that a flat z-vertex distribution and angular distribution is generated for correction reasons. The inaccurate position of the target has also been taken into consideration, making the Monte-Carlo events similar to the real data.

One of the most powerful tools for the data selection is the kinematic fit. The idea of kinematic fitting is to use the known constraints of a given physical process to improve the measurments describing the process. For example we can use mass constraints, energy constraints, etc.

3.1 Preselection

Before we can start an analysis, the data that we get has to be modified(selected) so that it will help us in our research. This is done to narrow down the number of entries that can be of use to us. Meaning instead of starting our analysis with 1000000 events we introduce some rough cuts that take out unwanted events, leaving us with example 100000 events as candidates for further research. Since we are looking at only neutral events and beam momenta of 900 MeV/c and 1800 MeV/c, the following steps are taken to remove unwanted events.

[1] **C**onfidence **L**evel

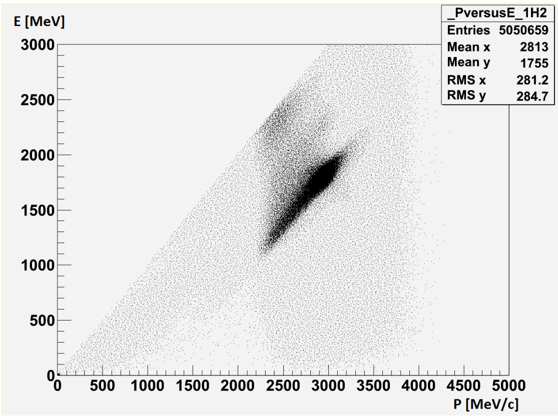

(a)

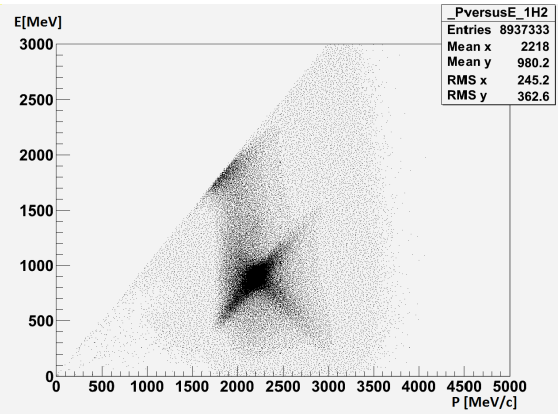

(b)

Figure 3.1: (a)Pvs.E (1800MeV/c) (b)Pvs.E (900MeV/c)

- All charged events are filtered out.
- Since we are looking at $\pi^0\eta \to 4\gamma$ and $\eta\eta \to 4\gamma$ channels only, any event that doesn't give us 4γ-s is removed.
- The momentum of the event will be limited through the help of Figure 3.1. For 900MeV/c an interval of ±500MeV/c is used and for 1800MeV/C an interval of ±400MeV/c.
- Events(refer to Fig. 3.1) in the energy range of 2219±800 MeV/c^2 for 900MeV/c and 3093±400 MeV/c^2 for 1800MeV/c have been selected.
- The interaction point of the $p\bar{p}$-annihilation should come from the target region.

After the preselection is done (Table 3.1) the events that remain are taken through another selection process (see section 3.5 - 3.6) and then are finally analysed.

	Detected events	Neutral Events	Momentum and Energy cuts	4-gamma events
Nr. of Events 900 MeV/c	88'485'380	8'937'333	7'493'106	486'712
Nr. of Events 1800MeV/c	67'971'450	5'050'659	4'598'808	252'363

Table 3.1: A statistical overview of the preselection

3.2 Kinematic Fit

For a given event hypothesis, measured as well as unmeasured quantities are supposed to fulfill certain kinematic constraints like energy and momentum conservation or invariant masses of particles. This allows the use of kinematic constraints leading to the improvement of data quality. The measured four vectors are within their error limits varied in such a way that the boundary conditions are fulfilled. Examples of these are the conservation laws of total energy and total momentum. Through this so-called kinematic fit the measured errors are reduced. For example if two photons are detected which is believed to have originated from an η decay. Then their momenta will be corrected till they can be traced to an η. However, the corrections must be kept to a minimum. For a fit, the total energy and total momentum of an event should agree with the following constraints:

$$\sum_{i=1}^{n} \vec{p}_i = \vec{p}_0 \tag{3.1}$$

$$\sum_{i=1}^{n} E_i = E_0 \tag{3.2}$$

Due to the uncertainties in the measured quantities, these constraints are not exactly fulfilled. The constraints can then be used to slightly change the measured values within their uncertainties. The concept of an event-by-event least square fitting together with the application of Langrange Multipliers can be utilized to ensure that the measured as well as unmeasured quantities fulfill the kinematic constraints deduced from the event hypothesis. This procedure is referred to as a kinematic fit. It not only results in a χ^2 test of the event hypothesis but also in improved estimators of the underlying kinematics for a given event.

$$\chi^2 = \sum_{i=1}^{n} \frac{\left(x_i - x_i^m\right)^2}{\sigma^2} = \sum_{i=1}^{n} \frac{\left(\delta y_i\right)^2}{\sigma^2} \tag{3.3}$$

Where x_i^m is the measured property and x_i is the fitted property. So now to complete the process the lagrange multipliers with constraints are introduced.

$$\sum_{k=1}^{n} \lambda_k f_k \left(\vec{y}, \vec{a}\right) \tag{3.4}$$

Adding the two equations (3.3) and (3.4) together will give:

$$L\left(\vec{y}, \vec{a}, \lambda\right) = \chi^2 + \sum_{k=1}^{n} \lambda_k f_k \left(\vec{y}, \vec{a}\right) \tag{3.5}$$

The optimal solution is found when χ^2 reaches a minimum and the total derivative $dL/dy = 0$. The unmeasured parameters can be calculated from the constraints, therfore we need more constraints than unmeasured parameters. If the constraints are linear then the solution can be directly calculated by the following equation.

$$\frac{\delta\chi^2}{\delta y_i} + \sum_{j=1} \frac{\delta f_i}{\delta y_i}\alpha_j = 0 \tag{3.6}$$

The confidence level CL provides information about how well the kinematic fit matches with physical hypotheses. The CL is only then minimal if χ^2 is maximal. One can separate the good events from the bad events by removing minimal CL-s. Mathematically the relation between χ^2 and the CL can be represented in the following way:

$$CL(\chi^2) = \int_{\chi^2}^{\infty} \frac{Z^{\frac{n}{2-1}} exp^{-\frac{z}{2}}}{2^{\frac{n}{2}}\Gamma(\frac{n}{2})} dz \tag{3.7}$$

Another variable is the so-called "pull" of the normalized shift in the measurement error of a measured value. If the measured values are Gaussian and their errors are precisely determined, then the pulls should exhibit a Gaussian distribution around the value 0 and they should have a width of 1.

3.3 Pulls for 900 MeV/c and 1800 MeV/c

The variables y_i in equation 3.3 characterize for every photon:

- ϕ : azimuthal angel of shower
- θ : polar angel of shower
- $\sqrt{E}$: square root of the energy of the shower

Since the measured properties are subject to certain fluctuations, the BCTRACK software cannot take into consideration the errors of the kinematic fit for the measured properties. The default values provided by the BCTRACK software must therfore be scaled with appropriate factors. This has been done with the pull distribution of the kinematic fits for the phase-space hypothesis. Ideally, the data distribution should have a Gauss form around 0 with a width of 1. The method for determining the scaling factors is an iterative process. Before the first iteration takes place reasonable scaling factors for $\phi, \theta, \sqrt{E}$ are chosen for the measurement. Then, starting from the given values the next best values are calculated. This process is repeated till the iteration converges in such a way that the χ^2 reached between the pull distribution and the ideal distribution is at a minimum. The iteration process had to be run for every momentum separately. The values are summarized in Table 3.2.

	900 MeV/c	1800 MeV/c
ϕ	0,8	1,0
θ	1,5	2,0
$\sqrt{E}$	0,6	0,6

Table 3.2: Scaling factors of the data

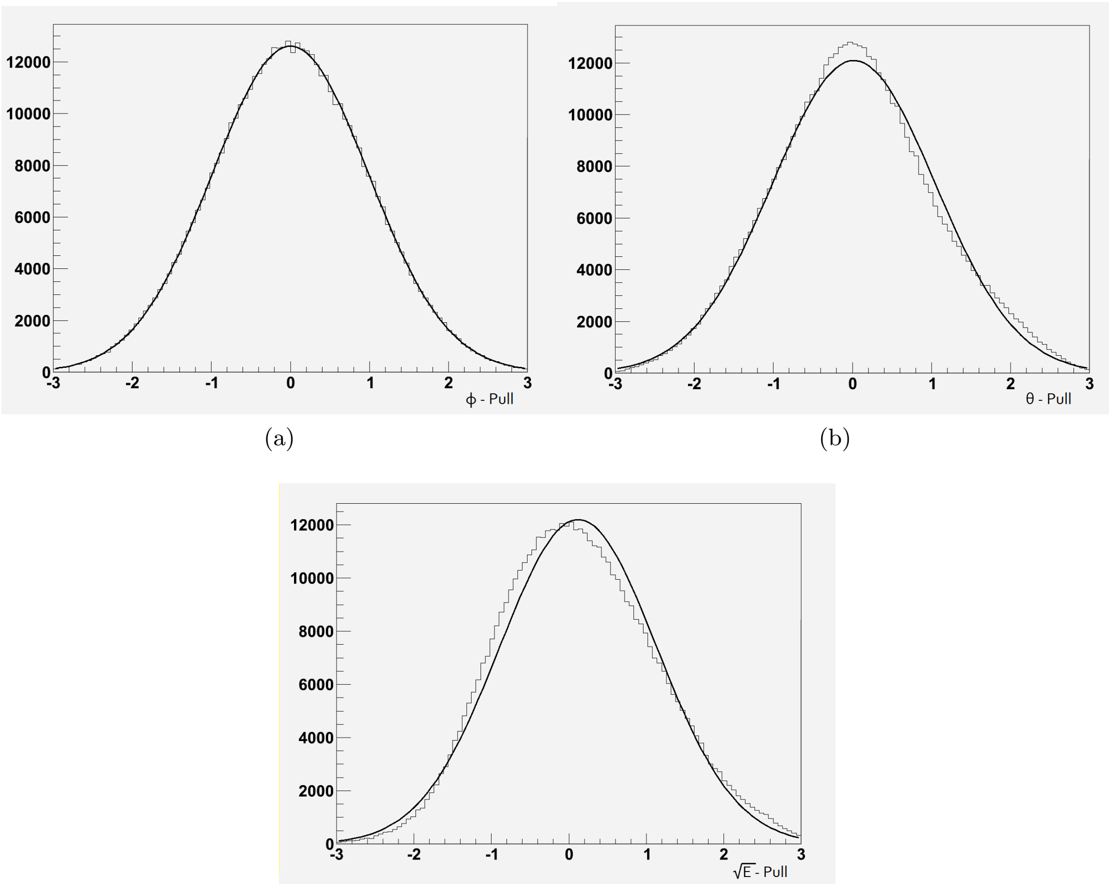

(a) (b)

(c)

Figure 3.2: (a)ϕ-coordinate (b)θ-coordinate (c)$\sqrt{E}$-coordinate for all a, b, and c $p = 900MeV/c$

With the obtained scaling factors a good Gaussian distribution for the pulls can be seen(Figures 3.2 and 3.3). The pull of the ϕ-coordinate is a very good approximation of a gaussian distribution for both momenta. The values of the gaussian distribution of the different pulls are summerized in Table 3.3. The mean value tells us how close the distribution is to zero, and the width of the distribution σ should be as close as possible to the value 1. The ϕ-coordinate has a mean value $\approx 0,0003$ for momentum 900 MeV/c

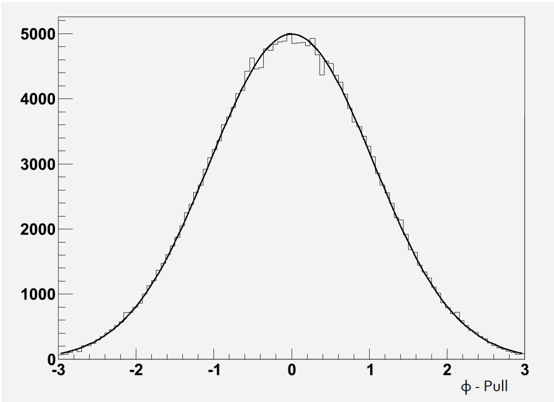

(a)

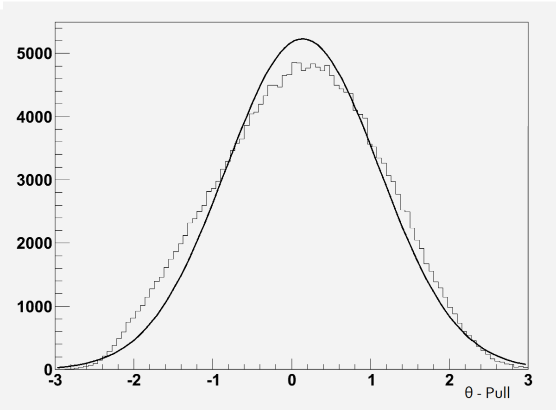

(b)

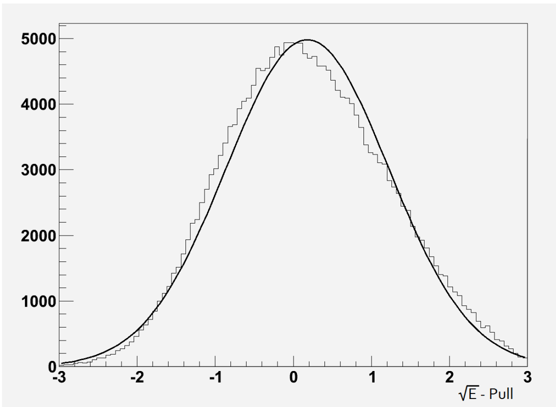

(c)

Figure 3.3: (a)ϕ-coordinate (b)θ-coordinate (c)$\sqrt{E}$-coordinate for all a, b, and c $p = 1800MeV/c$

and $\approx 0,0002$ for momentum 1800 MeV/c. Whereas the θ- and $\sqrt{E}$-coordinates of the 1800 MeV/c momentum are distributed more around the 0,1 to 0,2 values respectively. For the 900 MeV/c data the iteration proved to be more accurate and returned a mean value $\approx$ 0,02 for the θ-coordinate and 0,1 for the $\sqrt{E}$. The sigma represents as we know the length of the distribution, and since we are looking at gaussian distributions we should expect a value of 1(obviously it is hard to get the exact value 1).

Also The Monte Carlo events had to go through the iteration process. This was done using only the $\pi^0\pi^0$-Monte Carlo events. The results for both momenta are shown in Table 3.4 and you can see the pulls in Figures 3.4 and 3.5.

	900 MeV/c		1800 MeV/c	
	Mean	σ	Meam	σ
ϕ - Pull	$3,28 \cdot 10^{-4}$	$9,92 \cdot 10^{-1}$	$1,91 \cdot 10^{-4}$	1,05
θ - Pull	$1,83 \cdot 10^{-3}$	1,03	$1,41 \cdot 10^{-1}$	0,97
$\sqrt{E}$ - Pull	$1,21 \cdot 10^{-1}$	1,02	$1,80 \cdot 10^{-1}$	1,04

Table 3.3: The Gaussian distribution values of the $\pi^0\pi^0$ pulls that are shown in Figure 3.2 and 3.3

	900 MeV/c	1800 MeV/c
ϕ	0,8	0,9
θ	1,7	2,5
$\sqrt{E}$	0,8	0,8

Table 3.4: Scaling factors of the $\pi^0\pi^0$ Monte-Carlo data

Looking at Figure 3.5 one can see that both θ and $\sqrt{E}$ coordinates are a little bit displaced. Instead of having a gaussian distribution around the 0 value we instead have the distribution around the 0.1 value. But the σ values are all ≈ 1. Whereas in Figure 3.4(900 MeV/c) all three coordinates are close to the mean value of 0, but deviate minimally from the σ value that should be equal to 1(in our case sometimes we get a value closer to 0.9). All Monte Carlo pull values can be seen in Table 3.5.

	900 MeV/c		1800 MeV/c	
	Mean	σ	Meam	σ
ϕ - Pull	$-2,55 \cdot 10^{-4}$	1,10	$1,60 \cdot 10^{-4}$	1,02
θ - Pull	$7,32 \cdot 10^{-2}$	0,94	$1,11 \cdot 10^{-1}$	1,01
$\sqrt{E}$ - Pull	$1,21 \cdot 10^{-2}$	0,92	$1,41 \cdot 10^{-1}$	0,96

Table 3.5: The Gaussian distribution values of the $\pi^0\pi^0$ pulls that are shown in Figure 3.4 and 3.5

3.4 Applied Hypotheses

For the preparation of the final states $\pi^0\eta$ and $\eta\eta$ six hypotheses for the kinematic fit have been applied as follows:

1. $\bar{p}p \to \gamma\gamma\gamma\gamma$ (phasespace)
2. $\bar{p}p \to \pi^0\gamma\gamma$, where $\pi^0 \to \gamma\gamma$
3. $\bar{p}p \to \pi^0\pi^0$, where each $\pi^0 \to \gamma\gamma$

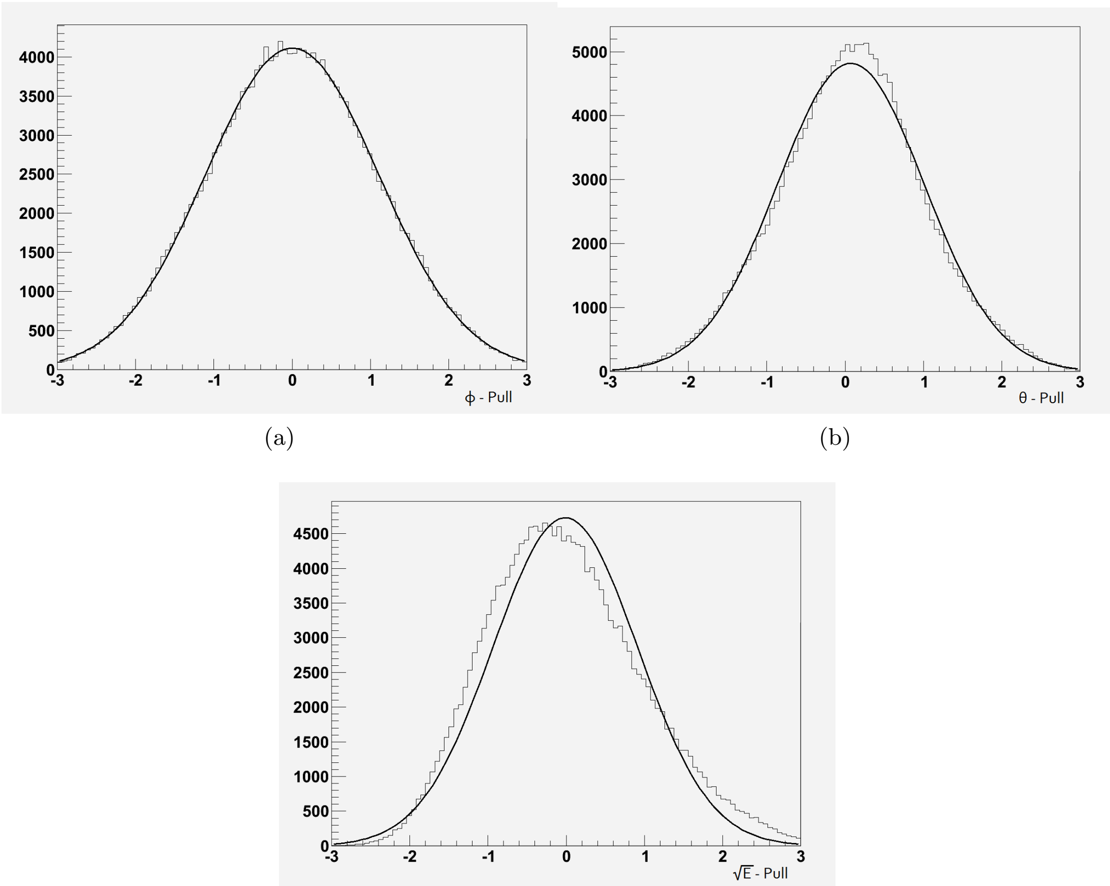

(a) (b) (c)

Figure 3.4: (a)ϕ-coordinate (b)θ-coordinate (c)$\sqrt{E}$-coordinate
For all a, b , and c $p = 900MeV/c$ Monte-Carlo events

4. $\bar{p}p \to \pi^0\eta$, where $\pi^0 \to \gamma\gamma$ and $\eta \to \gamma\gamma$
5. $\bar{p}p \to \eta\eta$, where each $\eta \to \gamma\gamma$
6. $\bar{p}p \to \pi^0\eta'$, where $\pi^0 \to \gamma\gamma$ and $\eta' \to \gamma\gamma$

The two hypotheses that are of great intrest are (4) and (5). These two final states will be examined in the section below. The selection of the 4γ-s that correspond to these hypotheses is done by applying cuts on the CL-s of the different channels. Ideally the CL-s should be flat for all events that satisfy the corresponding hypotheses (which means having a total flat CL between the values 0 and 1). Figure 3.6 showes that the CL-s of the phasespace, $\pi^0\eta$, and $\eta\eta$ have a peak that streches all the way till the estimated value of 0.1 (10%). This is due to background and wrongly reconstructed events. The main background channel for $\pi^0\eta$ ($\eta\eta$) is the $\pi^0\pi^0$ ($\pi^0\eta$) respectively. The

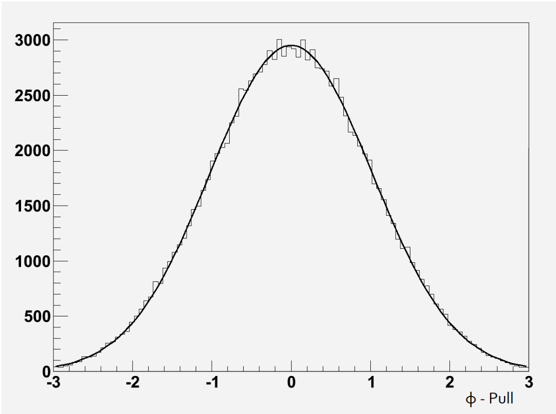

(a)

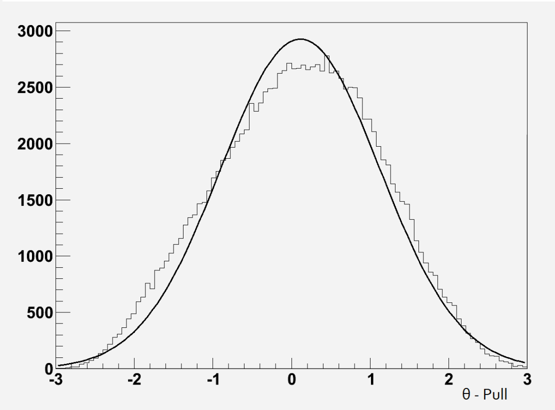

(b)

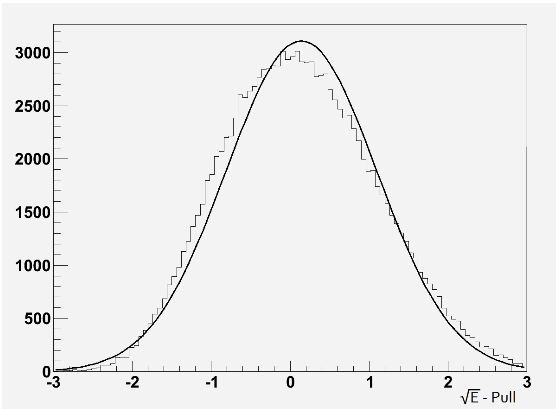

(c)

Figure 3.5: (a) ϕ-coordinate (b) θ-coordinate (c) $\sqrt{E}$-coordinate For all a, b, and c $p = 1800MeV/c$ Monte-Carlo events

wrongly reconstructed events are mainly events with a missing gamma (due to one gamma escaping the detector without being detected). For example $\pi^0\omega$ decays to 5γ-s (see Table 1.1), but refering to Figure 3.7 it is clear that when the invariant mass of the first $\gamma\gamma$-pair versus the invariant mass of the second$\gamma\gamma$-pair is drawn. It can be seen that between the $\pi^0\eta$ and $\pi^0\eta'$ events. There are a lot of events being detected. These are the $\pi^0\omega$ events that have been wrongly reconstructed as 4-γ events.

3.5 Selection Criteria of $\pi^0\eta$

In order to minimize events from the other channels, the selection of the $\pi^0\eta$-channel takes place using Monte-Carlo data. For that we need to simulate all the other channels ($\pi^0\pi^0$, $\eta\eta$, $\pi^0\eta'$, and $\pi^0\omega$). The goal here is to select in such a way that a minimum number of events from the other channels pass the selection criteria, but at the same

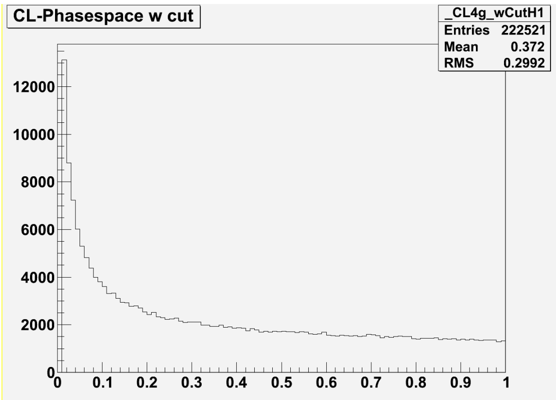

(a) CL-phasespace 900MeV/c

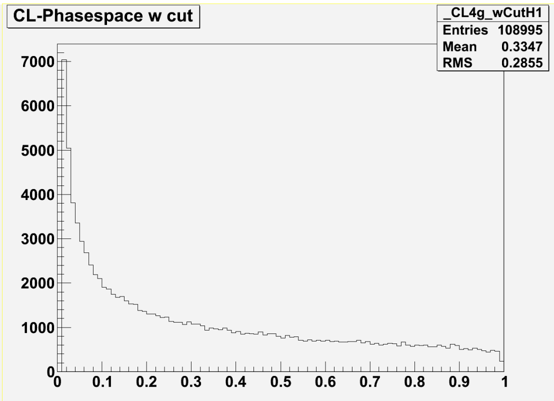

(b) CL-phasespace 1800MeV/c

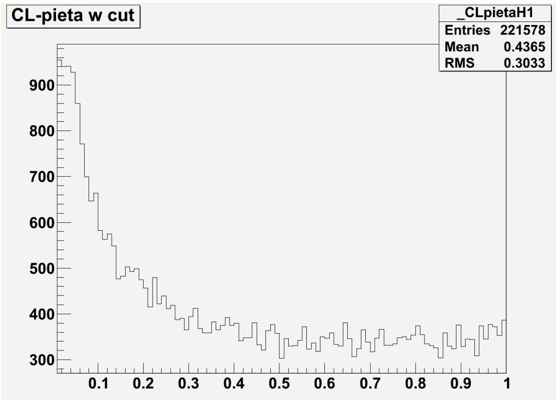

(c) CL-$\pi^0\eta$ 900MeV/c

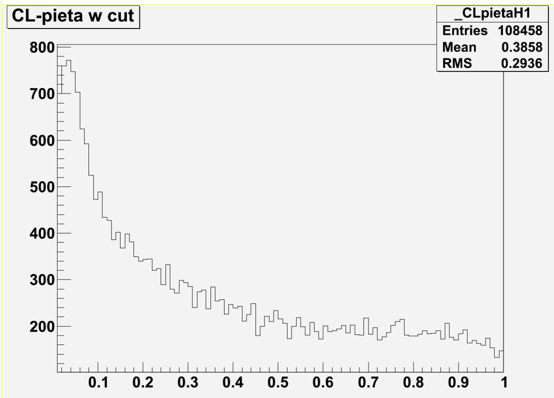

(d) CL-$\pi^0\eta$ 1800MeV/c

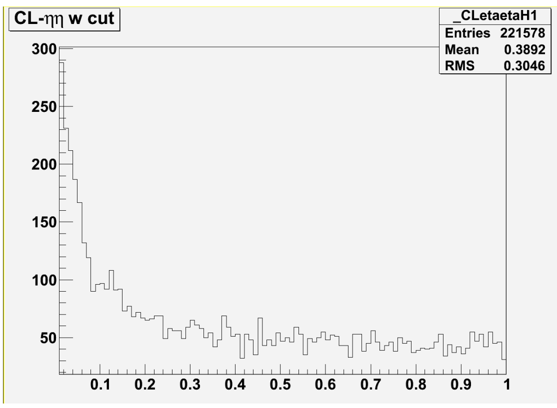

(e) CL-$\eta\eta$ 900MeV/c

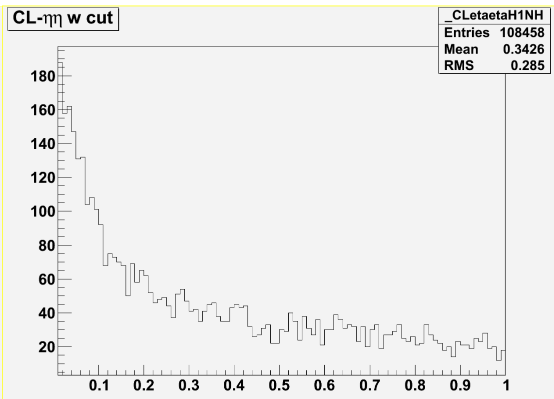

(f) CL-$\eta\eta$ 1800MeV/c

Figure 3.6: The CL-s of the phasespace, $\pi^0\eta$, $\eta\eta$

time loose as few as possible signal events ($\pi^0\eta$-events). Therfore CL cuts are optimized by creating a diagram where the CL of $\pi^0\eta$ vs. the other channels (see Figure 3.8) are

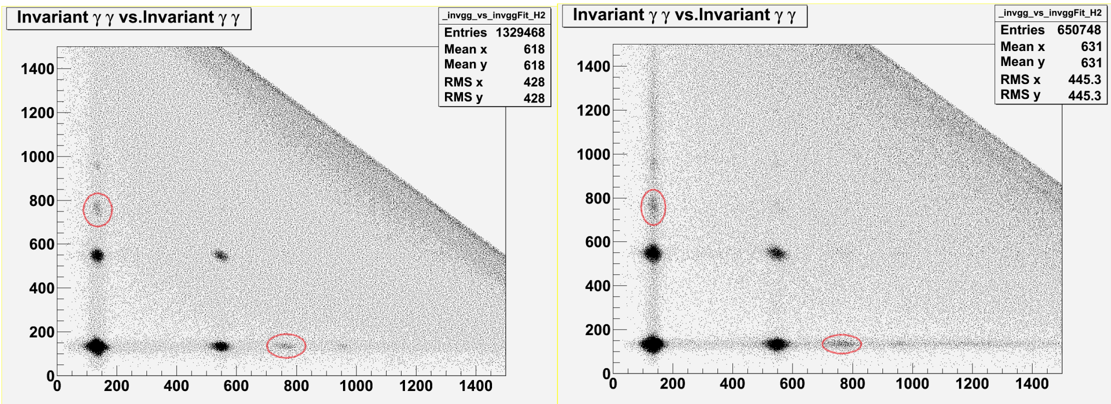

(a) (b)

Figure 3.7: (a) invariant $\gamma\gamma$ mass vs invariant $\gamma\gamma$ mass of a 900MeV/c beam (b) invariant $\gamma\gamma$ mass vs invariant $\gamma\gamma$ mass of a 1800MeV/c beam the red circle shows a distribution of $\pi^0\omega$ events.

plotted.

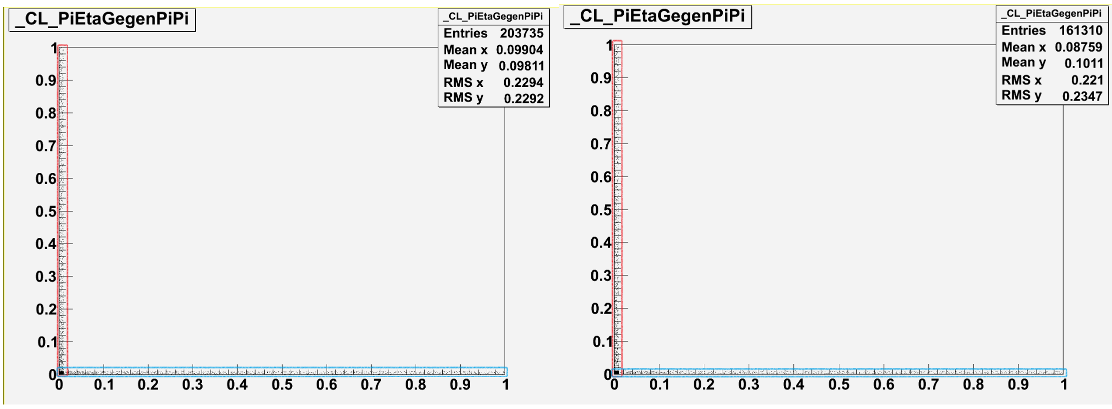

(a) $CL(\pi^0\eta)$ vs. $CL(\pi^0\pi^0)$ for 900 MeV/c (b) $CL(\pi^0\eta)$ vs. $CL(\pi^0\pi^0)$ for 1800 MeV/c

Figure 3.8: the red box shows where all the $\pi^0\eta$ events are and the blue box the $\pi^0\pi^0$events

By looking at Figure 3.8 it is clear that a $CL(\pi^0\pi^0) < 0,01$ cut can be applied to get rid of almost all the $\pi^0\pi^0$ events and yet keep a maximum number of $\pi^0\eta$ events. With this method the cuts can be optimized. The CL of the $\pi^0\eta$ was also cut to get an almost flat CL, but it was difficult to decide where the cut should be. When a cut of 20% was applied there were a lot of events that were lost although they were $\pi^0\eta$ events. At 10% there was too much background for the 1800 MeV/c beam, so with a cut right at the middle the results were acceptable. For the 900 MeV/c a cut at 10% proved to be acceptable the background was minimal and not a lot of $\pi^0\eta$ events were discarded in the process. The values obtained are in Table 3.6.

Channel	CL-Cut (900 MeV/c)	CL-Cut (1800 MeV/c)
$CL(\pi^0\pi^0)$	$< 0,01$	$< 0,01$
$CL(\pi^0\eta)$	$> 0,1$	$> 0,15$
$CL(\eta\eta)$	$< 0,01$	$< 0,01$
$CL(\pi^0\eta')$	$< 0,01$	$< 0,01$

Table 3.6: CL cut values for the different channels ($\pi^0\eta$ is the main signal)

These cuts were applied to get a statistical overview of how many entries make it through from all the channels. Table 3.7 shows that a large number of the signal events survive all the cuts, whereas the background events are reduced to a minimum.

Main channel / Background Channel	1800 MeV/c	900 MeV/c
	$\pi^0\eta$	$\pi^0\eta$
$\pi^0\pi^0$	57	11
$\pi^0\eta$	35968	45620
$\eta\eta$	1	7
$\pi^0\eta'$	4	5
$\pi^0\omega$	173	98

Table 3.7: Statistical overview of events that remain after selection cuts are applied for $\pi^0\eta$.

The values in Table 3.7 have been obtained using 100000 Monte-Carlo events per channel for the 1800 MeV/c beam and 200000 events for the 900 MeV/c beam. After the pre-selection around 40000 events were left (1800 Mev/c) and around 50000 events for the 900 MeV/c momentum beam. So the cuts did not remove a significant amount of the main channel, but almost all events from the background channels were discarded. The reconstruction efficiency of the main signal for 1800 MeV/c is 36, 0% and for the 900 MeV/c momentum 22, 8%. Leaving an acceptable data sample to analyse the angular distribution of $\pi^0\eta$.

3.5.1 Angular Distribution of $\pi^0\eta$

The angular distribution should be a symmetric distribution along the z-axis (forward-backward) in the center of mass. Figure 3.9 shows the angular distributions at both (900 and 1800 MeV/c) momenta of the $\pi^0\eta$ without correction for acceptance. Then the Monte Carlo generated angular distribution is divided through a simulated flat angular distribution. Yielding the efficiency (Figure 3.10). Finally the sample data (measured using the detector) is divided by the efficiency, yielding the final corrected angular distribution as shown in Figure 3.11.

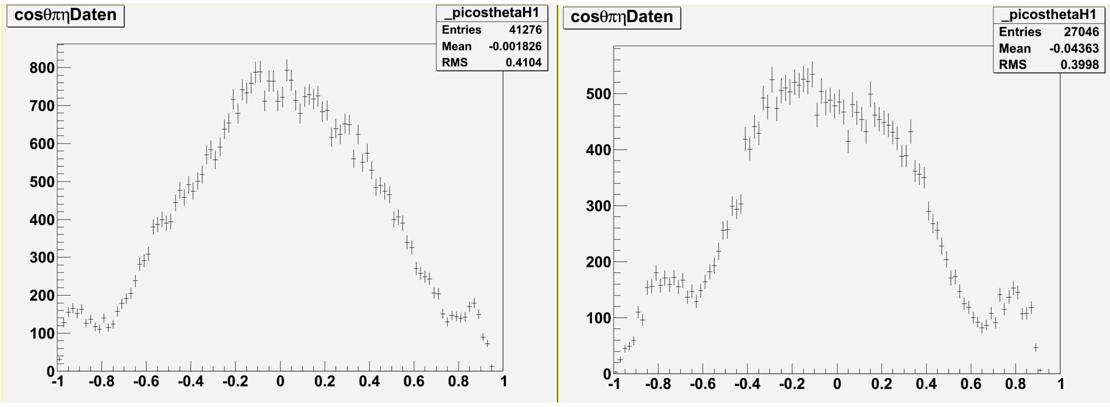

(a) 900 MeV/c (b) 1800 MeV/c

Figure 3.9: Angular distribution of data uncorrected

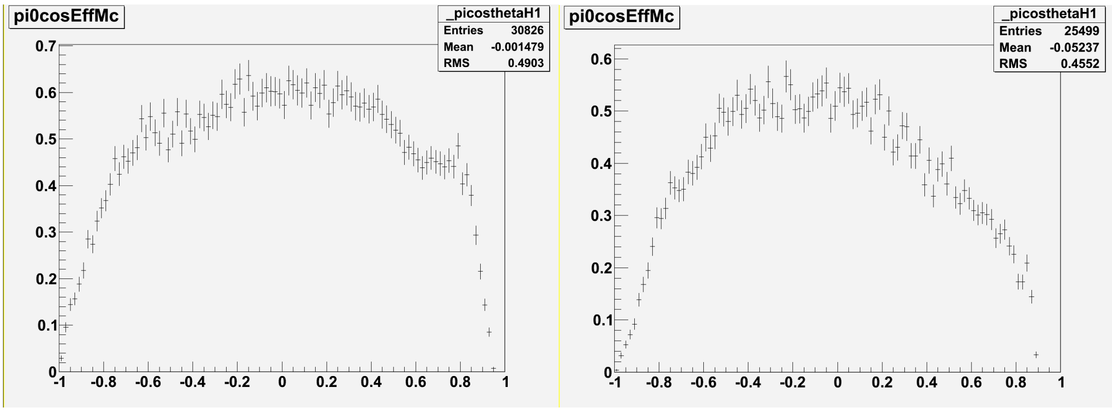

(a) 900 MeV/c (b) 1800 MeV/c

Figure 3.10: The reconstruction efficiency of $\pi^0\eta$ obtained from MC

Figure 3.11 shows a clear symmetry at 0. At certain points there are slight irregular asymmetries, but that might be due to the fact that the EMC crystals have a finite size, and that causes the software to reconstruct the entries at the center of the crystals instead of spreading them out uniformly across it's surface (limited resolution). This does not cause a significant change on the conclusions drawn.

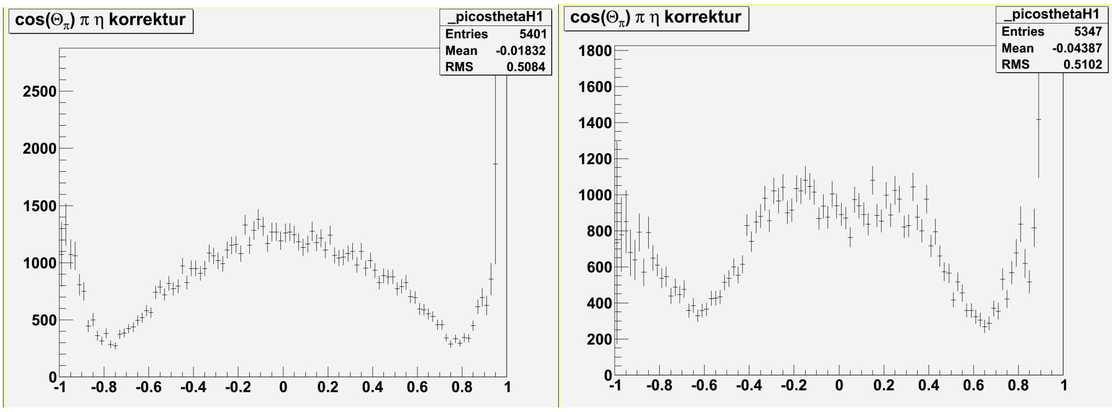

(a) 900 MeV/c (b) 1800 MeV/c

Figure 3.11: Angular distribution of data corrected

3.6 Selection Criteria of $\eta\eta$

The selection criteria is analogous to the $\pi^0\eta$, except now we are selecting $\eta\eta$ events and minimizing the number of events of the other channels coming through. So just like in section 3.4 a diagram will be created that will show where the cut can be made on the CL-s of the background channels (Figure 3.12). The main background channel here is the $\pi^0\eta$.

After the cuts are applied (Table 3.5). Only $0,001\%$ of $\pi^0\eta$-events remain (900 MeV/c) and $0,009\%$ of the events remain when the beam momentum is at 1800 MeV/c, since there are no cuts applied to the $\pi^0\omega$ events. More of them remain($0,03\%$) than the $\pi^0\eta$ events.

The $\eta\eta$ channel has an advantage that the $\pi^0\gamma\gamma$ hypothesis can be completely filtered out, because 4γ events that give 2 η-s are needed. So one can use this to remove $\pi^0\pi^0$ and $\pi^0\eta$ events without loosing many $\eta\eta$ events. The cuts that were performed are shown in Table 3.8, and in Table 3.9 we have a statistical overview of how many events actually passed through. For the 900 Mev/c 200000 Monte-Carlo events were used, so the reconstruction efficency is $29,4\%$ for the 1800Mev/c beam and $17,0\%$ for the 900 Mev/c both percentages are less than the reconstruction efficency of the $\pi^0\eta$. There are two ways of looking if the reconstruction took place correctly. One method is by looking at the invariant mass of the first$\gamma\gamma$-pair vs. the inariant mass of the second$\gamma\gamma$-pair. The other method is to first reconstruct from two γ-s an η and then plot the other two γ-s in an $\eta\gamma\gamma$ diagram and finally apply cuts till we have only one peak remaining at around 547 MeV. In this paper only the first method will be used. In Figure 3.12 we can see the final cut applied on each channel and what changes they cause. These cuts are applied on the real data now. At the top right corner we have the number of entries which we need to divide through 6 to get the real number of events, because we have 6 different combinations of the four γ-s. The cut order that was used to get the data in Figure 3.12 is as follows: first the $\pi^0\pi^0$ events were removed. Then the $\pi^0\eta$ events were taken out.

After that the $\pi^0\eta'$ events were removed. Finally the final cut around the $\eta\eta$ events was applied to get a flat CL. The figure includes the phasespace and $\eta\eta$ cuts done only on the 900 Mev/c momentum beam, but the same process was used on the 1800 MeV/c beam too.

Channel	CL-Cut (900 MeV/c)	CL-Cut (1800 MeV/c)
$CL(\pi^0\gamma\gamma)$	$< 0,1$	$< 0,1$
$CL(\pi^0\pi^0)$	$< 0,01$	$< 0,01$
$CL(\pi^0\eta)$	$< 0,01$	$< 0,01$
$CL(\eta\eta)$	$> 0,1$	$> 0,1$
$CL(\pi^0\eta')$	$< 0,01$	$< 0,01$

Table 3.8: CL cut values of the different channels (for $\eta\eta$)

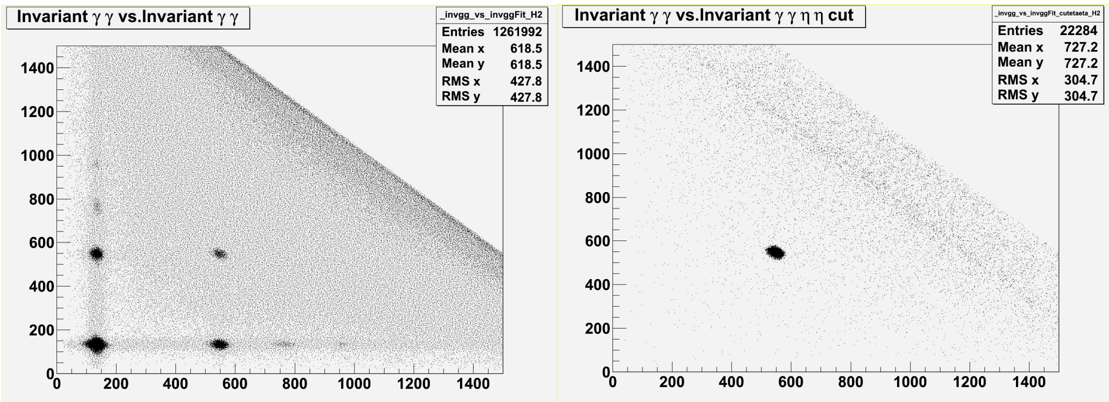

(a) inv $\gamma\gamma$ mass vs. inv $\gamma\gamma$ mass phase space cut

(b) inv $\gamma\gamma$ mass vs. inv $\gamma\gamma$ mass $\eta\eta$ cutt

Figure 3.12: (a) is the phase space cut (b) the final cut to $\eta\eta$ is applied

3.6.1 Angular Distribution of $\eta\eta$

The angular distribution should show symmetry in the z-axis. This symmetry can be seen in Figure 3.13, which are the diagramms of the uncorrectred angular distributions. Figures 3.14 and 3.15 show us respectively the reconstruction efficiency and the corrected angular distribution.

Background Channel \ Main channel	1800 MeV/c	900 MeV/c
	$\eta\eta$	$\eta\eta$
$\pi^0\pi^0$	1	1
$\pi^0\eta$	9	2
$\eta\eta$	29364	33919
$\pi^0\eta'$	1	2
$\pi^0\omega$	30	19

Table 3.9: Selection cuts applied to get $\eta\eta$ events

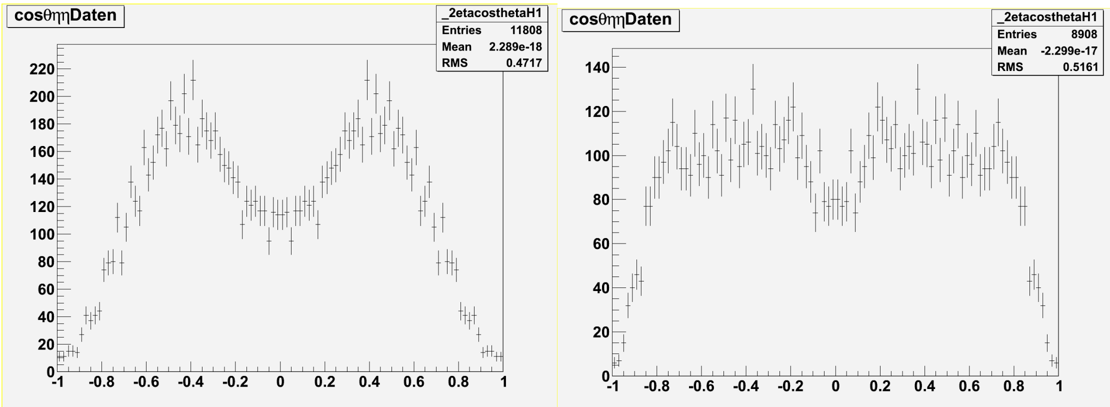

(a) 900 MeV/c (b) 1800 MeV/c

Figure 3.13: The angular distribution of $\eta\eta$ without the acceptance correction

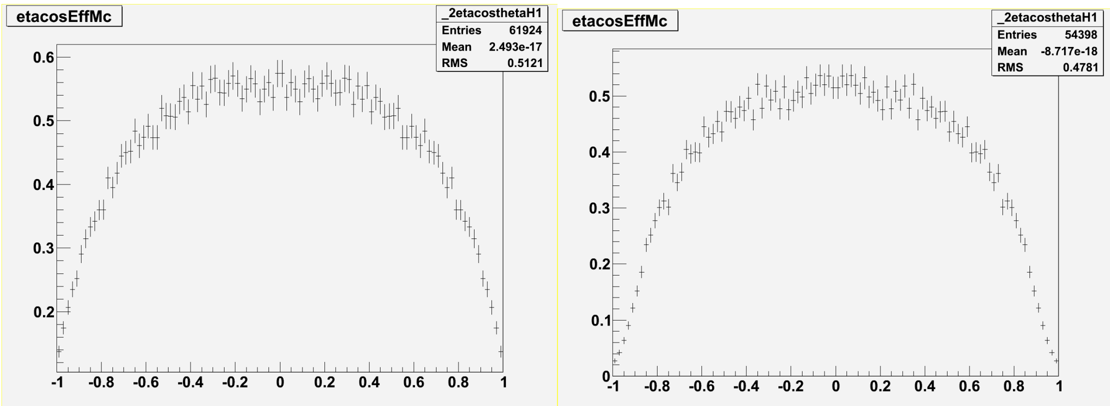

(a) 900 MeV/c (b) 1800 MeV/c

Figure 3.14: The reconstruction efficancy of $\eta\eta$

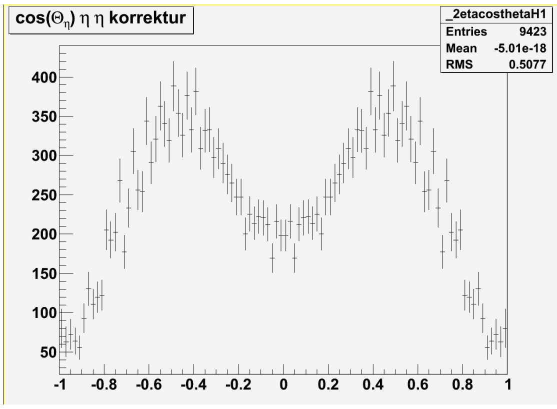

(a) 900 MeV/c

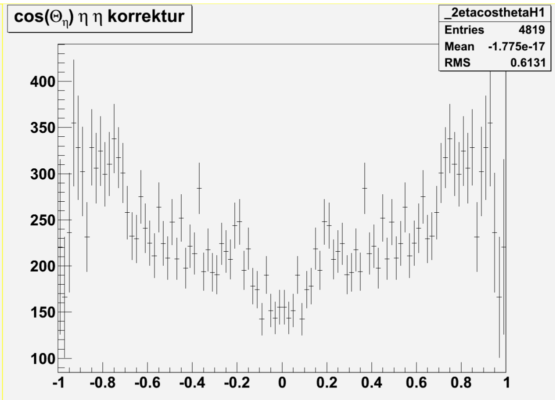

(b) 1800 MeV/c

Figure 3.15: The angular distribution of $\eta\eta$ with the acceptance correction

4 Summary

The Angular distribution of the two channels $\pi^0\eta$ and $\eta\eta$ are compared to the papers written by A. Sarantsev and D.V. Bugg [10, 11]. It is easy to see that the results of this thesis are very similar to that of A. Saranatsev and D.V. Bugg. The only major differences are the number of Monte Carlo events generated, the software versions, and the energy scalings. These cause the results to be more precise. In this thesis we generate for 1800 MeV/c 100'000 events and for 900 MeV/c 200'000, whereas A. Saranatsev and D.V.Bugg use only 20'000 events. The high number of Monte Carlo events generated, leads to less fluctuations in the Angular distributions. That is why with 100'000 and 200'000 events more accurate angular distributions can be reconstructed.

List of Tables

List of Figures

Bibliography

[1] D. Lange, Nucl. Instrum. Methods Phys. Res., Sect. A462, 152 (2001)

[2] (04.97) A. Berdoz, C.A. Meyer, W. Röthel and P. Schmidt Report on the last Crystal Barrel Runs: October through December 1996.

[3] (06.95) LOCATOR user manual for version 2.00/00 and a users guide is also available http://www-meg.phys.cmu.edu/cb/manuals.html

[4] (01.95) BCTRACK user manual http://www-meg.phys.cmu.edu/cb/manuals.html

[5] (04.95) GTRACK user manual for version 1.34/00 http://www-meg.phys.cmu.edu/cb/manuals.html

[6] (02.92) CBGEANT Software Manual and a mini-guide is also available http://www-meg.phys.cmu.edu/cb/manuals.html

[7] (07.93) G. Folger 0ffline reconstruction software V1.22/04

[8] (09.93) P. Hidas Kinematic Fitting Software V2.14/00

[9] http://root.cern.ch/drupal/

[10] (10.98) A. Sarantsev and D.V. Bugg. Antiproton-proton Annihilation $\rightarrow \eta\eta$ and $\eta\eta'$ from 600 to 1940 MeV/c.

[11] (11.98) A. Sarantsev and D.V. Bugg. Antiproton-proton Annihilation $\rightarrow \eta\pi^0$ and $\eta'\pi^0$ from 600 to 1940 MeV/c.

Acknowledgement

I want to thank Prof. Dr. Ulrich Wiedner who has given me the opportunity to write this thesis. I also want to thank Dr. Torsten and Julian for the help that they provided. A special thanks goes to my parents who have supported and encouraged me throughout this period and to Dr. Bertram Kopf who stood by me and helped me put this thesis together. Thank you Johnny (MS) and Alex for all the help and support. Finally i want to thank the whole faculty of experimental physics I for the friendly atmosphere.